

Particle motion in a liquid film rimming the inside of a partially filled rotating cylinder

D.D. Joseph, J. Wang, R. Bai, B.H. Yang
Department of Aerospace Engineering and Mechanics
University of Minnesota, Minneapolis, MN 55455

H.H. Hu
Department of Mechanical Engineering and Applied Mechanics
University of Pennsylvania, Philadelphia, PA 19104-6315

August 2002

Abstract

Both heavier- and lighter-than-liquid particles will float on liquid-air surfaces. Capillary forces cause the particles to cluster in typical situations identified here. This kind of clustering causes particles to segregate into islands and bands of high concentrations in thin liquid films rimming the inside of a slowly rotating cylinder partially filled with liquid. A second regime of particle segregation, driven by secondary motions induced by off-center gas bubbles in a more rapidly rotating cylinder at higher filling levels, is identified. A third regime of segregation of bidisperse suspensions is found in which two layers of heavier-than-liquid particles that stratify when there is no rotation, segregate into alternate bands of particles when there is rotation*.

I. Capillary forces

The deformation of the air-liquid interface due to floating light particles or due to trapped heavy small particles gives rise to capillary forces on the particles. These forces may be qualitatively understood from simple arguments. Two kinds of forces act on particles: forces due to gravity and forces due to the action of contact angles. These two kinds of forces are at play in the vertical force balance but require a somewhat more elaborate explanation for horizontal force balance. The effects of gravity are usually paramount for heavier-than-liquid floating particles in which one particle will fall into the depression of the second. A heavier-than-liquid particle will fall down a downward sloping meniscus while an upward buoyant particle will rise. Capillary forces cause particles to cluster as shown in figure 1.

* Movies of the experiments reported in this paper can be viewed at the web address <http://www.aem.umn.edu/research/particles/rtcylinderpaper/>.

In this section, we shall review the nature of capillary forces which cause the particles to cluster; in section II we show how these forces produce islands and bands of segregated particles in a thin liquid film rimming the inside of a slowly rotating cylinder.

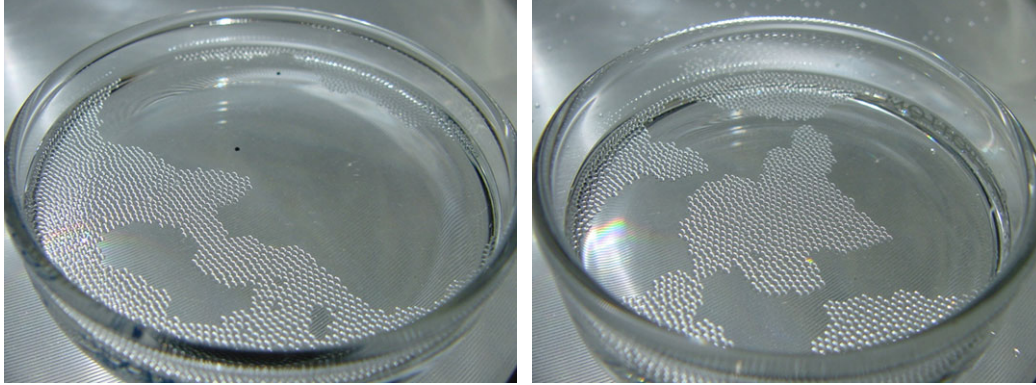


Figure 1. Neutrally buoyant glass beads cluster in water.

I-1. Vertical forces

The simplest analysis relevant to understanding the forces on small particles is the vertical force balance on a sphere floating on the interface between fluids which, for convenience, is here called water and air. This analysis was given first by Princen (1969), then by Rapacchietta and Neumann (1977) and by Kotah, Fujita and Imazu (1992), who used the floating ball to measure contact angles.

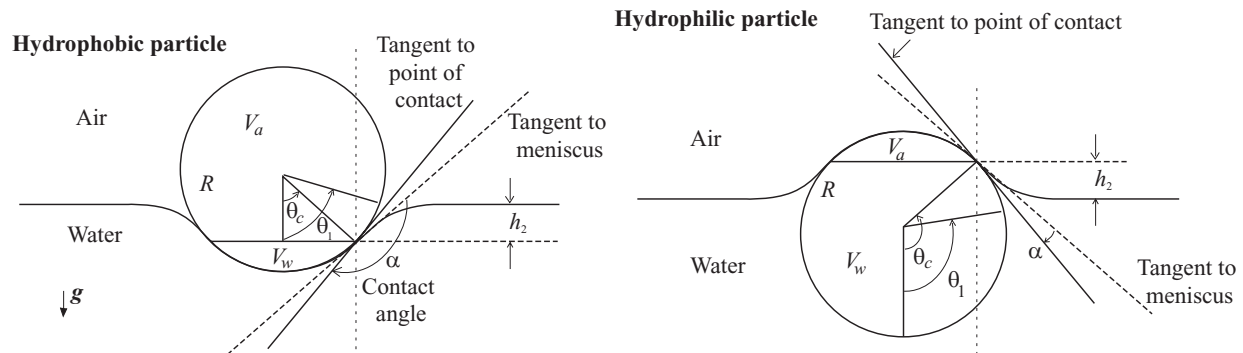


Figure 2. Hydrophobic and hydrophilic particles at equilibrium. The position of the contact ring is determined by θ_c . The point of extension of the flat meniscus on the sphere is given by θ_1 .

The capillary force F_c , is a function of the radius of particle R , the surface tension coefficient γ , the filling angle θ_c and the contact angle α (see figure 2), given by,

$$F_c = 2\pi(R \sin \theta_c)\gamma \sin[\theta_c - (\pi - \alpha)] = -2\pi(R \sin \theta_c)\gamma \sin(\theta_c + \alpha) \quad (1)$$

for both the hydrophobic case and the hydrophilic case.

To have mechanical equilibrium, the capillary force plus the vertical resultant of pressure around the sphere must balance the gravity vertical component,

$$F_c + F_p = G \quad (2)$$

where $G = \frac{4}{3}\rho_p\pi R^3 g$ is the weight of the particle, and the vertical resultant of pressure around the sphere can be written as

$$F_p = \rho_l g \pi R^3 \left(\frac{2}{3} - \cos \theta_c + \frac{1}{3} \cos^3 \theta_c \right) + \rho_a g \pi R^3 \left(\frac{2}{3} + \cos \theta_c - \frac{1}{3} \cos^3 \theta_c \right) - (\rho_l - \rho_a) g h_2 \pi R^2 \sin^2 \theta_c \quad (3)$$

where ρ_l and ρ_a are densities of the liquid and the air, respectively. Using the fact that $V = \frac{4}{3}\pi R^3$ is the volume of the sphere, $V_w = \pi R^3 \left(\frac{2}{3} - \cos \theta_c + \frac{1}{3} \cos^3 \theta_c \right)$ is the volume of the sphere immersed in the water and $A = \pi R^2 \sin^2 \theta_c$ is the area of the ring of contact, we can rewrite (3) as,

$$F_p = \rho_l g V_w + \rho_a g (V - V_w) - (\rho_l - \rho_a) g h_2 A. \quad (4)$$

The first two terms at the right hand side are in agreement with Archimedes' principle, while the term $(\rho_l - \rho_a) g h_2 A$ accounts for the meniscus effect. When a meniscus is present, the buoyancy calculated by Archimedes' principle $\rho_l g V_w + \rho_a g (V - V_w)$ not only lifts the sphere, but also the fluid in the meniscus. Hence, we need to subtract the weight of the lifted fluid from $\rho_l g V_w + \rho_a g (V - V_w)$ to get the buoyancy on the sphere. Expression (4) implies that the volume of the lifted fluid is $h_2 A$.

Inserting (1) and (3) into (2), we get the vertical force balance,

$$\sin \theta_c \sin(\theta_c + \alpha) = -\frac{B}{2} \left[\frac{4}{3} \psi_1 - \left(\frac{2}{3} - \cos \theta_c + \frac{1}{3} \cos^3 \theta_c \right) - \psi_2 \left(\frac{2}{3} + \cos \theta_c - \frac{1}{3} \cos^3 \theta_c \right) + (1 - \psi_2) (\cos \theta_c - \cos \theta_1) \sin^2 \theta_c \right] \quad (5)$$

where $B = \rho_l R^2 g / \gamma$ is the bond number and $\psi_1 = \rho_p / \rho_l$ and $\psi_2 = \rho_a / \rho_l$ are the dimensionless control parameters.

It can be inferred from (5) that the left side of the equation, consequently, the right side, lies in the range $-1 \leq \sin \theta_c \sin(\theta_c + \alpha) \leq 1$. Obviously this equation cannot be solved if the particles are too large or too heavy. We can also conclude that:

Small particles can be suspended in fluid surfaces no matter how heavy they may be provided $\rho_p R^2 g / \gamma \rightarrow 0$. Moreover, in this limit $\sin \theta_c \sin(\alpha + \theta_c) = 0$ and the particles sit on top of the fluid or are held in place by capillarity.

If the particle is irregular with sharp corners the capillarity argument fails. Liquid-air surfaces bind at razor sharp corners; the physics associated with this strong bond are not understood. Razor blades and straight pins can float on water-air surfaces pinned at the sharp surface.

Equation (5) suggests that hydrophobic nanoparticles can float on the surface no matter how heavy they are. However, even though the formula does not predict that hydrophilic particles will sink, they will sink because of a not-understood wetting instability. If heavy nanoparticles are put into the liquid, they will not rise. The surface layer on a liquid which gives rise to surface tension is very small, but not zero; likewise, the concept of contact angles on nanoparticles may lose meaning.

I-2. Horizontal forces

The deformation of a liquid-fluid interface due to trapped small particles gives rise to lateral capillary forces exerted on the particle. A simple explanation is shown in figure 3. A heavier-than-liquid particle will fall down a downward sloping meniscus while an upwardly buoyant particle will rise.

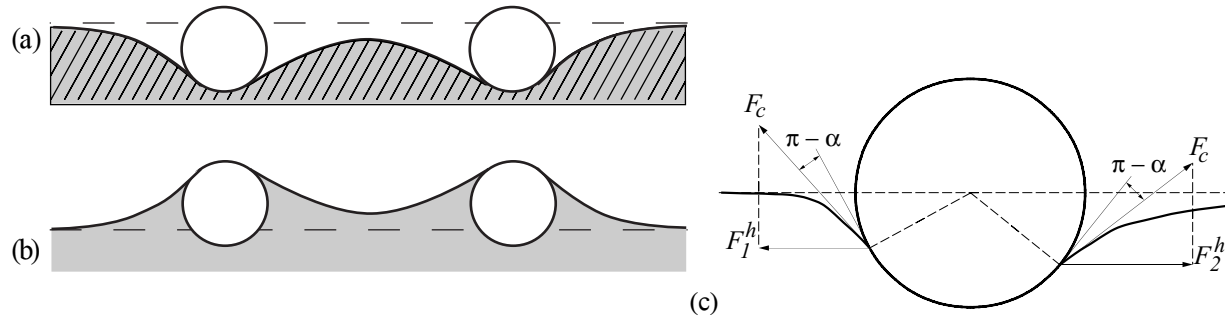


Figure 3. Spherical particles in water, (a) heavier-than-water hydrophobic particles. The meniscus is below the undisturbed level. If the contact angle doesn't vary the particle must tilt causing an imbalance of the horizontal component of capillary forces pulling the spheres together. Even if the particles do not tilt they will both fall under gravity into the depression between them. (b) Lighter-

than-water hydrophilic particles will rise into the elevated section of the meniscus and come together. The meniscus is above the undisturbed level. (c) If for any reason, the particle tilts with the two contact angles equal, a horizontal force imbalance will result. In the figure, the vector F_c indicates the magnitude of the capillary force and F_1^h and F_2^h are horizontal components, $F_2^h > F_1^h$.

There are several ways to isolate the effects of capillarity uninfluenced by gravity. Poynting and Thompson (1913) investigated the capillary effect by considering two vertical plates immersed in a liquid, the space between the plates is a two dimensional capillary tube. If the plates are hydrophobic, the level in the capillary gap sinks below the liquid outside; if the plates are hydrophilic the levels will rise. Their argument about the nature of horizontal forces on the plates is given in the caption of figure 4. Repulsion between particles with different wetting properties is rather short range because it stops when the meniscus between particles gets flat.

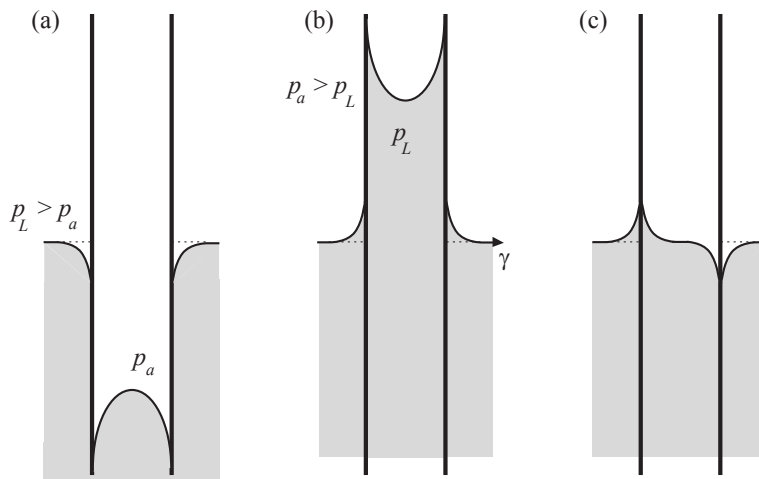


Figure 4. (After Poynting and Thompson 1913). Horizontal forces associated with the fall (a) of liquid between hydrophobic plates and the rise (b) of liquid between hydrophilic plates. In (c) one plate is hydrophilic and the other hydrophobic. The contacts on both sides of a plate are the same and the tension γ is constant. They argue that the net horizontal force due to γ can be calculated at flat places; so that there is no net horizontal component of the tension. In (a) and (b) the pressures are such that they push the plates together; there is no net attractive force in (c). If the plates (c) are so close that there is no flat place, then the horizontal projection $\gamma \sin \alpha$ of the interface midway between the plates is smaller than the horizontal component outside the plates and the plates are pulled apart; they repel. They note that "... small bodies, such as straw or pieces of cork, floating on the surface of a liquid often attract each other in clusters; this occurs when the bodies are all wet by the liquid and also when none of them is wet; if one body is wet and one is not wet, they repel each other." (It may help here to note that if one face of the plate is hydrophobic and the other hydrophilic, the contact angles will put the plates in tension, tending to pull them apart.)

Another way to take away the effects of gravity is to support the particles on a substrate. In this case the horizontal forces are due to capillary effects alone. Katoh, Fujita and Imazu (1992) studied the motion of a particle floating on a liquid meniscus which could be interpreted as motion on a substrate because the foaming polystyrol particles used by them are an order of magnitude lighter than water, and minimize the effects of gravity compared to capillarity. Their experimental results are completely consistent with the predictions of Poynting and Thompson (1913): when the sphere and the wall are alike with respect to wetting; say both are hydrophobic or hydrophilic, the wall and sphere attracts; when they are unlike the sphere and wall repel.

Despite the well-established importance of the capillary meniscus forces there are only a few theoretical works devoted to them. Nicolson (1949) was the first to derive an analytical expression for the capillary force between two floating bubbles by using the superposition of approximation to solve the Laplace equation of capillarity. A similar approximate method was applied by Chan, Henry and White (1981) to floating spheres and horizontal cylinders. For horizontal cylinders the alternative approaches were proposed by Gifford and Scriven (1971) and by Fortes (1982). The theoretical works are based on solutions of the Laplace equations for capillary menisci of translational or rotational symmetry, where the Laplace equation reduces to an ordinary differential equation.

An analytical solution of the Laplace partial differential equation in bipolar coordinates was proposed by Kralchevsky, Paunov, Ivanov and Nagayama (1992), and Kralchevsky, Paunov, Denkov, Ivanov and Nagayama (1993) for the case of small particles and small meniscus slope. This solution provides expressions for calculating the capillary meniscus force between two vertical cylinders, between two spheres partially immersed in a liquid layer and between a vertical cylinder and a sphere. A review is recently presented by Kralchevsky and K. Nagayama (2000).

Their theory (see Kralchevsky and Nagayama, 2000), which has been validated in experiments, provides the following asymptotic expression for calculating the lateral capillary force between two particles of radii R_1 and R_2 separated by a center-to-center distance L ,

$$F = -2\pi \gamma Q_1 Q_2 q K_1(qL) \left[1 + O(q^2 R_k^2) \right] \quad \text{when } L \gg r_k \quad (6)$$

where $r_k = R_k \sin \theta_c$ ($k=1$ and 2) are the radii of the two contact lines (see figure 2);

$$Q_k = r_k \sin \psi_k \quad (k=1 \text{ and } 2) \quad (7)$$

with ψ_k being the meniscus slope angles with respected to the horizontal plane at the contact point ($\psi > 0$ for floating light particles, and $\psi < 0$ for heavy particles);

$$q = \sqrt{(\rho_l - \rho_a)g/\gamma} \quad (8)$$

is the inverse of the capillary length; in addition $K_1(x)$ is the modified Bessel function of the first order. The expression (6) is valid for particles much smaller than the capillary length ($q^{-1} = 2.7\text{mm}$ for water-air interface).

I-3. Particle clustering

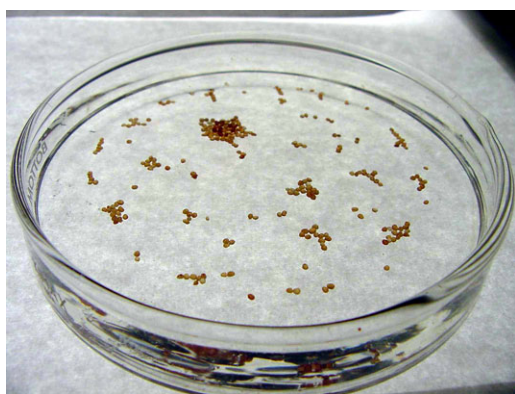
Due to the attractive lateral capillary forces between similar particles floating on a liquid surface, particles tend to cluster. The dynamic behavior of clustering is not well characterized. Gifford and Scriven (1971) noted that “casual observations... show that floating needles and many other sorts of particles do indeed come together with astonishing acceleration. The unsteady flow fields that are generated challenge analysis by both experiment and theory. They will have to be understood before the common-place ‘capillary attraction’ can be more than a mere label, so far as dynamic processes are concerned.”

There are a small number of theoretical studies of the drag and diffusion coefficient of a spherical particle attached to a fluid interface (Brenner and Leal 1978, 1982; Goldman, Cox and Brenner 1967; Schneider, O’Neill and Brenner 1973; Majumdar, O’Neill and Brenner 1974—which may be collectively designated as Brenner *et al*—and Wakiya 1957; Redoev, Nedjalkov and Djakovich 1992; Danov, Aust, Durst and Lange 1995). A recent study of Saif (2002) develops a theory of capillary interactions between solid plates forming menisci on the surface of a liquid.

The only experimental determination of drag coefficients for particles of any size were performed by Petkov, Denkov, Danov, Velev, Aust and Durst (1995) for particles of sub-millimeter radius by measuring the particle velocity under the action of well defined external force. They showed that the capillary interactions are quite strong and very long range. Accelerations, which are very great under many conditions of interest, have not been studied before.

We found that the initially randomly distributed particles floating on a liquid surface tend to cluster due to the attractive lateral capillary forces between the particles. It is generally observed

that the particles initially form small clusters, then the small clusters slowly merge into bigger ones; and eventually the bigger ones are assembled into a giant cluster. This self-assembly process is shown in the pictures of figure 5. The procedure by which we obtain dispersions like those shown at 3 min in figure 5 is noteworthy. We create such dispersions by pouring particles on the liquid, nothing complicated, just like a salt shaker. As soon as the particles hit the liquid surface they disperse rapidly leading to dispersions like that at 3 min in figure 5. The dispersions then attract. This initial repulsion, followed by attraction, is more or less universal and we have not seen it mentioned in the literature.



Elapsed time: 3 minutes



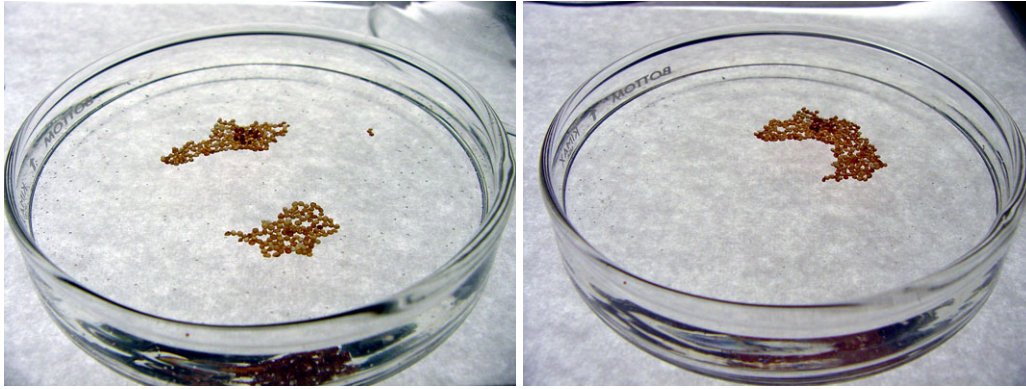
10 minutes



30 minutes



2 hours



12 hours

24 hours

Figure 5. Free motions leading to self-assembly of floating particles (sands in 1% aqueous polyox solution).

Experiments on particle clustering due to capillarity were carried out in glass petrie dishes with diameters ranging from 5 to 15 cm. Three different liquids (table 1) and two different hydrophobic particles (table 2) were used. Hydrophobic particles did not collect on the glass side-walls of the petri dishes so that end effects arising from walls in dishes of different sizes were not important.

Type of liquid	Glycerin	Soybean oil	Triton mixture
Density ρ (g/cm ³)	1.173	0.915	1.241
Viscosity μ (cp)	1490	282	2950
Surface Tension (mN/m) (measured with a spinning-drop tensiometer)	41.46	24.28	33.15

Table 1. Physical parameters for liquids.

Type of particle	Polymer particle	Nylon particle
Density ρ (g/cm ³)	1.034	1.170
Diameter d_p (cm)	0.065	0.314

Table 2. Physical parameters for particles.

Clustering, of the type shown in figure 5, was observed for both types of the particles in glycerin and in the Triton-water mixture. These particles could not be suspended in soybean oil, because they were too heavy. However, they could be held by capillarity in the hanging film shown in figure 8.

Rate of approach experiments were conducted for two identical particles attracted by capillary forces on the Glycerin-air and Triton mixture-air interface. The distance between the two particles was measured with a video camera as a function of time until they touch, as shown in figures 6 and 7. The curves are not similar near the time of final approach. During the final stages of approach, the approach velocity depends strongly on liquid properties. Particles in a 6000 cp Triton mixture barely move even when they are placed very close together. On the other hand, the rate of approach of hydrophobic particles on water-air surfaces is surprisingly fast in the final times. The approach velocity is smaller for the smaller particles, but the data was erratic and quantitative results were not obtained.

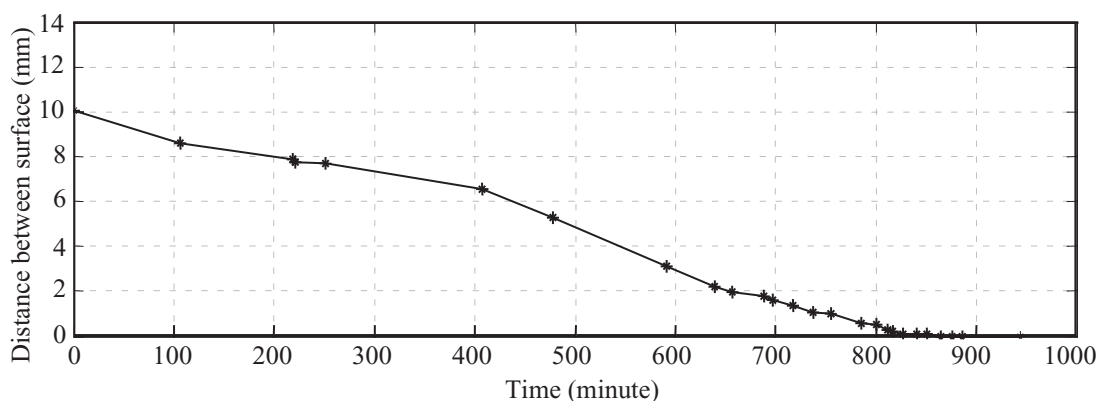


Figure 6. Distance between the two identical particles. Triton mixture (2950 cp) and nylon particles were used.

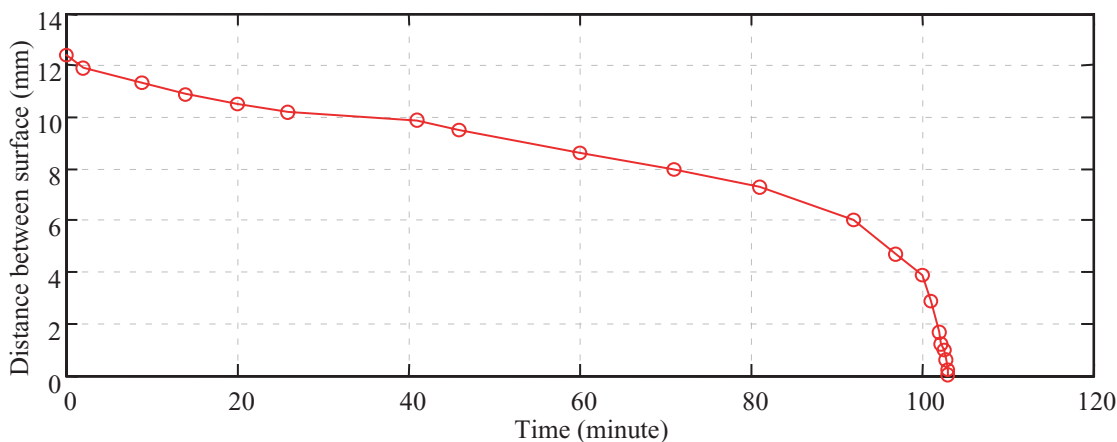


Figure 7. Distance between the two identical particles. Glycerin and nylon particles were used.

The photograph in figure 8 shows the aggregation of polymer particles in a hanging glycerin film on the bottom of a flat glass plate taken from the top of the plate. The particles are

encapsulated by glycerin and drawn together in hanging drops of glycerin robustly stable for months. This hanging drop configuration is shown in figure 10 as a cartoon in side view.

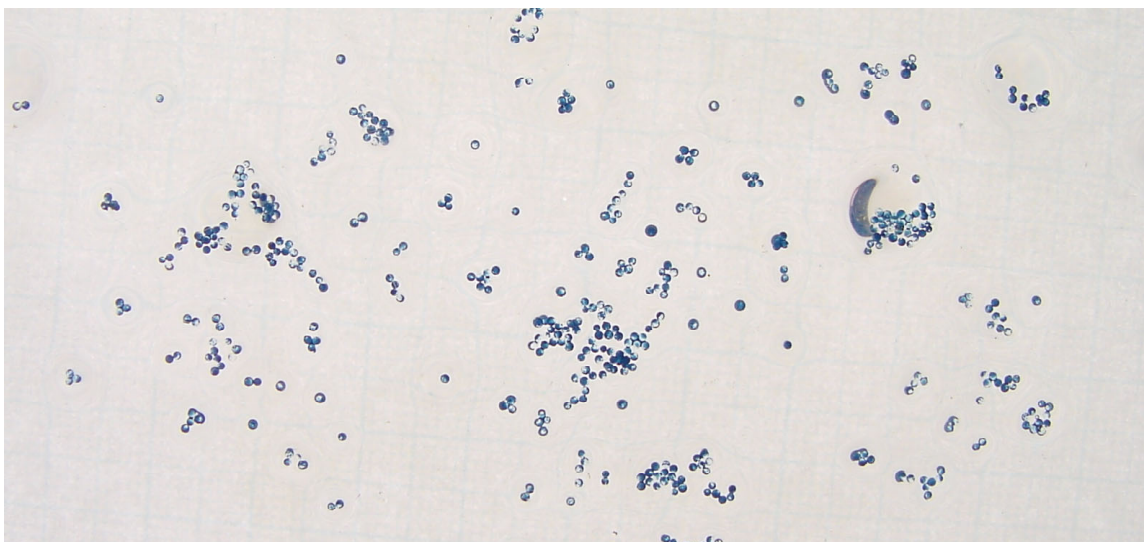


Figure 8. Aggregates of polymer particles in glycerin drops hanging from the bottom of a glass plate.

The ability of self-assembly of particles under the action of lateral capillary forces has been used by Whitesides *et al.* (1997, 1999, 2001). They assembled topologically complex mesoscale (from millimeter to micrometer size) objects into ordered two-dimensional arrays by floating the objects at the interface between perfluorodecalin (hydrophobic) and water. The structure of the arrays was manipulated by the design of the shape of the assembling objects and wettability of their surfaces. They modeled the self-assembly process as the minimization of the total interfacial free energy (the sum of the capillary energy and the gravitational energy) of the liquid-liquid interface.

II. Particle aggregation in a liquid film rimming a rotating cylinder

Tirumkudulu, Tripathi and Acrivos (1999) first reported particle segregation in a suspension of monodispersed neutrally buoyant spheres in a Newtonian liquid medium being sheared in a partially filled horizontal Couette device. They found that the suspension separates itself into alternating regions of high and low particle concentration along the length of the tube. In a following study, Tirumkudulu, Mileo and Acrivos (2000) (hereafter denoted as TMA 2000) observed that under certain circumstances particles which are initially uniformly mixed in a film rimming a horizontal rotating cylinder will also be drawn into cylindrical bands of high particle

concentration separated by regions of pure liquid. They did not offer a quantitative explanation of this phenomenon but suggested that the cause might be found in changes of the effective viscosity of the suspension induced by fluctuations of concentration. A theory relying on the shear induced diffusion of particles, concentration-dependent viscosity and the existence of a free surface was developed by Govindarajan, Nott and Ramaswamy (2001) to provide an explanation of the above mentioned experiments. However, quantitative comparison with the experimental data was not provided. A latest experimental result was reported by Timberlake and Morris (2002) in which concentration band dynamics was studied using a partially filled Couette device. They showed that the particle migration process observed in experiments was much faster than that predicated by the shear induced diffusion theory, about 40 times faster in one case examined, suggested strong evidence against shear-induced diffusion as the mechanism responsible for the observed segregation.

We carried out similar experiments and identified two regimes in which particles segregate; a low-speed, low-Reynolds number regime, in which particles are segregated at thin places on the rimming film by lateral capillary forces, and a high-speed regime associated with the formation of bubbles (Balmer 1970, Karweit and Corrsin 1975, Preziosi and Joseph 1988 among others). The segregation at low Reynolds numbers occurs in the parameter ranges similar to those studied by TMA 2000. The high-speed segregation has not been noted before.

II-1. The ratio of the minimum film thickness to the particle diameter

The segregation of particles due to capillarity occurs in the thin part of the film rimming the rotating cylinder near the top of the cylinder. The critical parameter for this appears to be the ratio D_{min}/d_p , where D_{min} is the minimum film thickness which is near the top of the cylinder to the side in which the gravity and the vertical component of rotation point downward (figure 9).

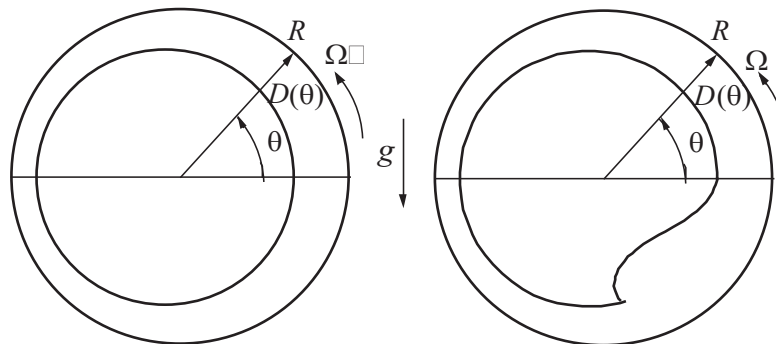


Figure 9. Film profile in rimming flow inside a rotating cylinder. (a) For small β . (b) For β larger than a critical value ($\beta_c = 1.414$).

We find that D_{min}/d_p is $O(1)$ and the rotational speed of the cylinder must be slow enough relative to the speed of capillary attraction to allow clusters to form more rapidly than they disperse in the pool of liquid at the bottom of the rotating cylinder. TMA (2000) identified the relevant rotation parameter

$$\beta = F \sqrt{\frac{gR}{\nu\Omega}} \quad (9)$$

where F is the fill ratio, i.e., the ratio of the total volume of liquid inside the cylinder to the volume of the cylinder; R is the radius of the cylinder; Ω is its angular rotational speed; ν is the kinetic viscosity of the liquid; g is the gravitational acceleration. The parameter β is the only dimensionless parameter to arise in lubrication theory; its relation to the filling parameter F is subtle and needs clarification. When $\beta < \beta_c = 1.4142$, a smooth film exists inside the rotating cylinder. However, when β is increased beyond the critical value β_c , smooth solution of the lubrication equations does not exist, and a bump is formed near the bottom of the cylinder where the film thickness varies rapidly, as is shown in figure 9 and in figures 1 and 3 of TMA (2000). Lubrication theory can be used to compute D_{min} when $\beta < \beta_c$; it can also be used to compute the minimum film thickness in the region above the pool of liquid when $\beta > \beta_c$ by a procedure which will be discussed below, but the solution is not uniformly around the cylinder in the pool below. The critical condition for the existence of a smooth solution of the lubrication equation for a thin film on the exterior of a rotating rod was called the “run-off” condition by Preziosi and Joseph (1988) and the critical condition for rimming flow was called a “run-on” condition. The run-off and run-on conditions were verified in experiment reported by Preziosi and Joseph (1988).

Many authors have published analyses of lubrication flows of liquids running inside of a rotating cylinder: Diebler and Cerro (1970), Moffatt (1977), Preziosi and Joseph (1988), Johnson (1988), O’Brien and Gath (1998) and Tirumkudulu and Acrivos (2001).

The segregation of particles by capillary forces does not correlate with β but the ratio D_{min}/d_p is important and lubrication theory can be used to compute D_{min} by the method described below. The physical parameters are the cylinder radius R , the kinematic viscosity of the fluid ν , the angular speed of rotation Ω , the volume fraction of the fluid F , the acceleration of gravity g , the

liquid flux Q , and the thickness of the film D . Preziosi & Joseph (1988) obtained the following equation for D using a lubrication theory:

$$Q = \Omega R D - \frac{g}{\nu} \frac{1}{3} D^3 \cos \theta = \Omega R D_0 - \frac{g}{\nu} \frac{1}{3} D_0^3 \quad (10)_1$$

where D_0 is the film thickness at $\theta = 0$. Let $h = D/R$ and $S = gR/\nu\Omega$, (10)₁ can be written in the following non-dimensional form:

$$\frac{Q}{\Omega R^2} = h - \frac{1}{3} S h^3 \cos \theta = h_0 - \frac{1}{3} S h_0^3 \quad (10)_2$$

where h_0 is the maximum film thickness; $h_0 = h(\theta)$ at $\theta = 0$ (see figure 9). Preziosi & Joseph gave the condition under which equation (10) is solvable:

$$h_0^2 S < 1. \quad (11)$$

Expression (11) is also the critical criterion of run-on.

O'Brien and Gath (1998) defined $\eta = D \left(\frac{g}{\Omega R \nu} \right)^{1/2} = \frac{D}{R} S^{1/2}$ and $q = Q \left(\frac{g}{\Omega^3 R^3 \nu} \right)^{1/2} = \frac{Q}{\Omega R^2} S^{1/2}$.

Under such definitions, (10) becomes:

$$q = \eta - \frac{1}{3} \eta^3 \cos \theta = \eta_0 - \frac{1}{3} \eta_0^3 \quad (12)$$

O'Brien and Gath gave the condition under which equation (12) is solvable:

$$0 < q < 2/3 \quad (13)$$

Note that when $q = 2/3$, the solution of (12) is $\eta_0 = h_0 S^{1/2} = 1$. Hence, the run-on criterion (11) is equivalent to (13).

The fluid fraction F can be computed by integrating $D(\theta)$:

$$F = \frac{1}{\pi R} \int_{-\pi}^{\pi} D(\theta) d\theta \equiv \frac{\beta}{S^{1/2}}, \text{ where } \beta = \frac{1}{\pi} \int_{-\pi}^{\pi} \eta(\theta) d\theta. \quad (14)$$

By virtue of (12) and (14), the value of β corresponding to $q = 2/3$ is $\beta = 1.4142$.

Therefore, the three run-on conditions are equivalent: $h_0^2 S < 1$, $0 < q < 2/3$, and $\beta < 1.4142$.

In our experiments, β is computed as $\beta = F S^{1/2} = F \sqrt{\frac{gR}{\nu\Omega}}$. When $\beta < 1.4142$, all the fluid join

the circulation. The fluid flux is obtained from F :

$$\frac{Q}{\Omega R^2} = \frac{F}{2} \quad (15)$$

Hence, equation (10) can be solved for $h(\theta)$ and the minimum film thickness is obtained.

The maximum film thickness h_o at $\theta = 0$ is an increasing function of β with a maximum at $\beta = \beta_c$. When $\beta > 1.4142$, there are places on the cylinder where the thickness of the layer is larger than the critical value, and the excess fluid will collect under the bump. However, it may be assumed that h_o remains at $\theta = 0$ (see figure 9); it is the maximum thickness of the film above the bump. This assumption could not be strictly correct; Ruschak and Scriven (1976) showed that under a perturbation of the thin film condition used to justify lubrication theory the position of the maximum thickness rotates into the first quadrant. It is probable that the assumption made here is reasonable but in any case we use it to calculate the value of D_{min} listed in table 3 when β calculated by equation (9) is greater than β_c .

The maximum film thickness that can be maintained by rotation is determined by the critical run-on condition (11), $h_o = 1/\sqrt{S} = \sqrt{\nu\Omega/gR}$. Therefore, we can calculate the actual fluid flux in the circulation by

$$\frac{Q}{\Omega R^2} = h_o - \frac{S}{3} h_o^3 = \frac{2}{3\sqrt{S}} \quad (16)$$

Then the minimum film thickness at $\theta = \pi$ is determined from the volume conservation (10),

$$\frac{Q}{\Omega R^2} = h_{min} + \frac{S}{3} h_{min}^3 = \frac{2}{3\sqrt{S}} \quad (17)$$

and is solved explicitly,

$$h_{min} = \frac{0.596072}{\sqrt{S}} = 0.596072 \sqrt{\frac{\nu\Omega}{gR}} \quad (18)$$

Corresponding to a specified filling level F , we may determine the average film thickness D_a from

$$F = \frac{\pi [R^2 - (R - D_a)^2]}{\pi R^2}, \text{ that is, } D_a = (1 - \sqrt{1 - F})R \quad (19)$$

II-2. Particle segregation in aqueous Triton mixtures

TMA 2000 found particle segregation in monodispersed sheared suspensions in a partially filled rotating horizontal cylinder when the filling fractions (liquid volume/total volume) were small $0.1 \leq F \leq 0.15$. The particle concentrations for the uniform mixtures were 5% and 15%. The values of β in experiments reported in TMA 2000 were all greater than β_c .

Systematic experiments on clustering of particles into bands were carried out using the polymer particle whose properties are described in table 2. In these experiments we used the same fluid as TMA. The liquid is a mixture of Triton X 100, ZnCl_2 and water in combinations used to control viscosity. The high viscosity mixture is in the range of 20-60 poise and a density in the range 1.1~1.5 g/cm^3 . The viscosity of the mixture is sensitive to temperature which was maintained at $68 \pm 2^\circ\text{F}$ in our experiments.

The experiments were conducted in two different rotating cylinders; one is 30 cm long and the inside diameter is 2.792 cm; the other is 15 cm long with the same inside diameter. The cylinder is supported horizontally and is driven at constant rotational speed Ω by a motor. For these experiments, the Reynolds number $R_e = (\Omega D_a^2)/\nu$, where Ω is the angular velocity of the cylinder, D_a the mean thickness of the film, and ν the kinetic viscosity of the fluid, is always very small (less than 10^{-2}). Inertial effects were generally negligible.

	F	R (cm)	Ω (rpm)	μ (poise)	ρ (g/cm^3)	ν (cm^2/s)	β	D_a (cm)	D_{min} (cm)	D_{min}/d_p
TMA 1	0.150	1.270	1.40	40.00	1.172	34.13	2.36	0.099	0.0480	1.04
TMA 2	0.125	5.000	2.80	49.00	1.172	41.81	2.50	0.323	0.149	3.24
M1	0.151	1.396	1.65	51.95	1.241	41.86	2.08	0.110	0.0605	0.931
M2	0.140	1.396	1.65	29.50	1.332	22.15	2.05	0.101	0.0440	0.677
M3	0.150	1.396	1.10	51.95	1.241	41.86	2.53	0.110	0.0494	0.760
M4	0.145	1.396	10.9	48.50	1.212	40.02	2.11	0.105	0.0966	1.49
M5	0.061	1.396	1.76	44.34	1.203	36.86	0.87	0.043	0.0403	0.620
M6	0.061	1.396	3.13	44.34	1.203	36.86	0.65	0.043	0.0412	0.634
M7	0.061	1.396	6.00	44.34	1.203	36.86	0.47	0.043	0.0418	0.648
M8	0.061	1.396	10.0	44.34	1.203	36.86	0.37	0.043	0.042	0.646
M9	0.046	1.396	38.71	2.377	1.498	1.587	0.67	0.032	0.0310	0.477
M10	0.046	1.396	51.10	2.377	1.498	1.587	0.58	0.032	0.0313	0.482

Table 3. Parameters for experiments reported in TMA (2000) and for our experiments (M1 through M10).

In table 3 we listed the parameters for the experiments using Triton mixtures reported by TMA and our experiments using the polymer particles (table2) colored blue for visualization. The particles used by TMA1 and TMA2 were neutrally buoyant with density 1.172 g/cm^3 , and diameter $d_p = 0.04625 \pm 0.00375 \text{ cm}$ in concentrations of 5% and 15%. In our experiments, M1-M10, the density of the particles $\rho_p = 1.034 \text{ g/cm}^3$ is less than fluid density; the diameters of the particles are more dispersed with an average particle diameter $d_p = 0.065 \text{ cm}$. The concentrations of the particles range from 2% to 7%. The cylinder length is 15 cm from M4 and M5; otherwise the cylinder length is 30 cm. The values of the minimum film thickness, D_{\min}/d_p , listed in table 3 are all of $O(1)$, and are consistent with the observations of particle segregation driven by capillarity of the thin films.

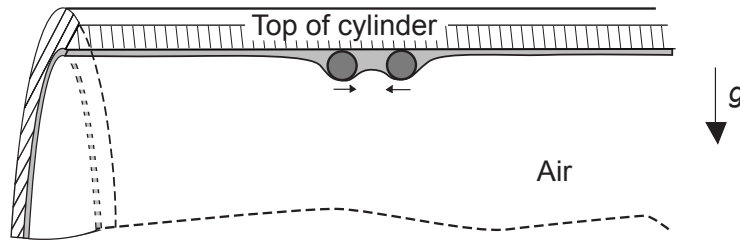
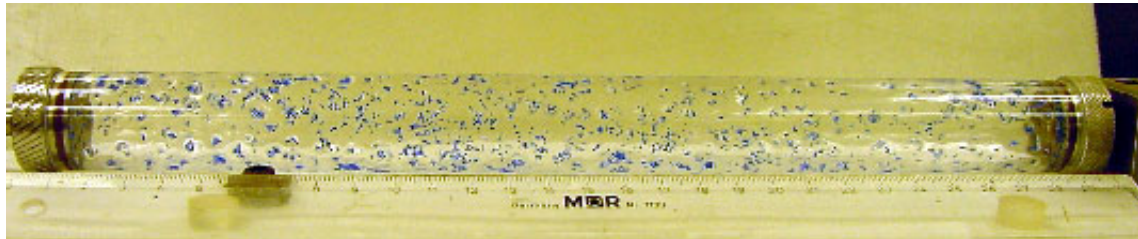


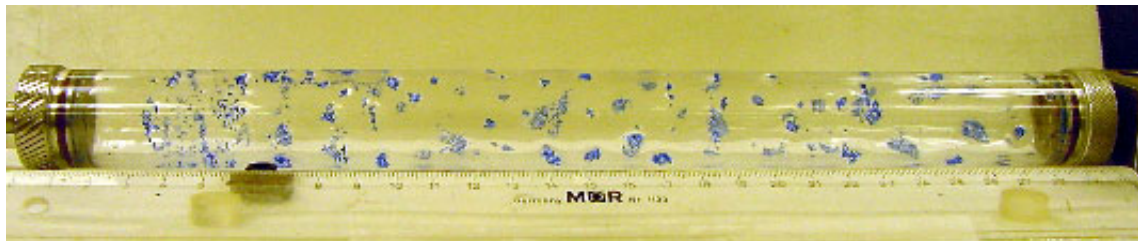
Figure 10. Capillary attraction of two particles hanging in a film at the top of a stationary rotating cylinder. The liquid film is the top section (the gray area). The air fills the other space.

After the cylinder is partially filled with the uniform suspension, it is turned a few times by hand and then put to rest so that the suspension covers the whole inside cylinder. It was observed that particles trapped in the thin film at the top of the cylinder move rather rapidly together under the action of capillarity (see figure 10). A similar kind of dynamics prevails when the cylinder rotates continuously at a constant velocity. In general the trapped particles are completely wet by the liquid as they pass through the deep pool at the bottom of the rotating cylinder. The segregation of particles generally occurs slowly. It takes a long time (hours) for the particles to reach the final steady band formation. The particle segregation occurs in a number of stages. The first is the formation of many small particle clusters, which were nucleated randomly along the cylinder after a few minutes. As time passes by, small particle clusters merge into larger ones. Eventually they form into several comparatively large blocks which are often far from each other. These large blocks are quite stable, and stay separated. Meanwhile, they are gradually stretched thinner and longer in the flow direction, and eventually form cylindrical bands. Some

bands may merge. The final formation of the bands is frequently uniform along the cylinder axis. The bands are not robustly stable; they may born, move, break and reform. It can be said that uniform dispersion is robustly unstable and clusters are robustly stable. The snap shots of the particle band formation are shown in figure 11.



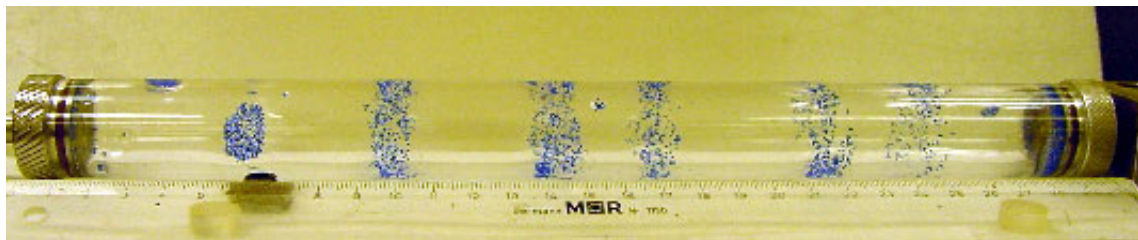
(a) Uniform distribution of particles at the beginning



(b) Particle clusters



(c) Larger clusters



(d) Particle bands

Figure 11. Process of particle bands formation. The experiment is performed with high viscous Triton-mixture fluid under low rotating speed and low filling level (case M7).

In our experiments, it is observed that the formation of particle clusters or bands is easier in more viscous liquid at a low rotational speed. In experiments with a high-viscosity Triton mixture, we had to restrict to low rotating speed to get bands to separate. The rotational speed of

the cylinder has to be slow enough such that the time needed for capillary attraction is comparable to the residence time for the particles in the thin part of the rimming film.

For the low-viscosity Triton mixtures, it is possible to get band separation by decreasing the filling level and at the same time increasing the rotational speed. The band formation was observed for the range of small β values (0.5~0.7). However, the rotational speed should not be too high, since then the particle clusters may not form, and even if particle clusters form they are not stable. The process of particle segregation in low-viscosity Triton mixtures (shown in figure 12) is similar to the case with high-viscous Triton-mixture (figure 11). Decreasing the filling level F as well as increasing the rotating speed is not always effective for low-viscosity fluids; we repeated the experiment with soybean oil and glycerin with relatively high rotating speeds (corresponding to $\beta=1.0\sim 1.2$), and even though bands did not form, particle clusters were always generated by capillary induced “anti-diffusion”.

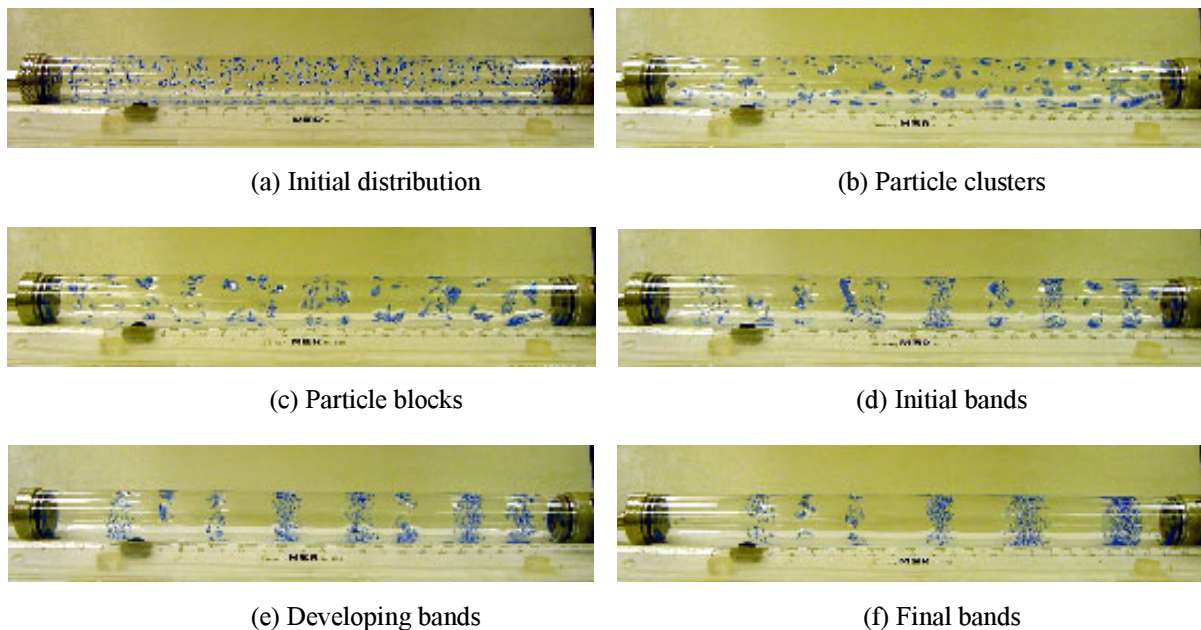


Figure 12. Process of particle bands formation. The experiment is performed with low viscous Triton-mixture fluid under relatively high rotating speed and low filling level (case M10).

Experiment M3 (table 3) is a high filling level case. Band separation occurred, however, there were many particles in the liquid sections between particle bands, in contrast to the case with low-filling where clear pure liquid between the particle bands were observed. The segregation of particles into cylindrical bands may take hours even days. The achieved

configurations are stable for times of the order of hours and days. There is slight secondary flow and transverse movement of particles can be seen between particle bands.

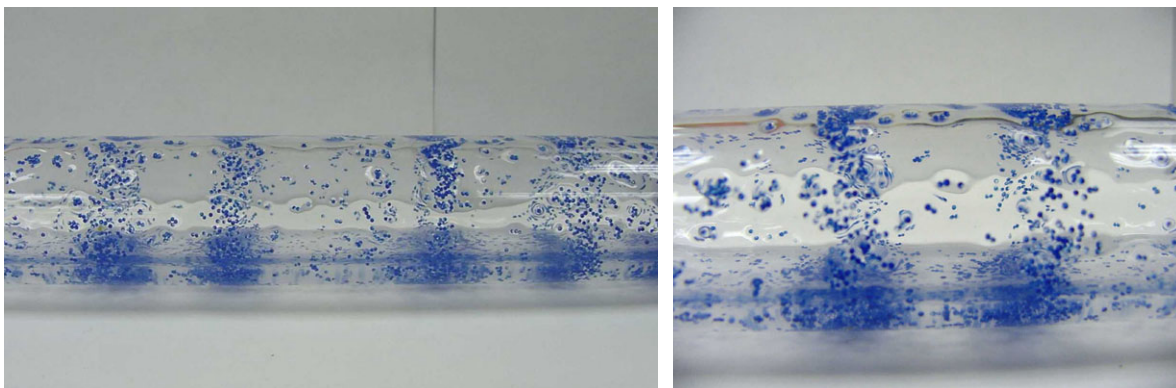


Figure 13. Particles which are initially distributed uniformly in a film rimming a rotating cylinder segregate into cylindrical bands (case M3). The formation of the bands takes hours.

In table 4, we list values for the times of formation of small clusters t_{w1} , large clusters (called blocks) t_{w2} and bands t_{w3} and the distance between bands as a function of the filling level and angular velocity. In general, for the same filling level, clusters form faster with the rotational speed increasing.

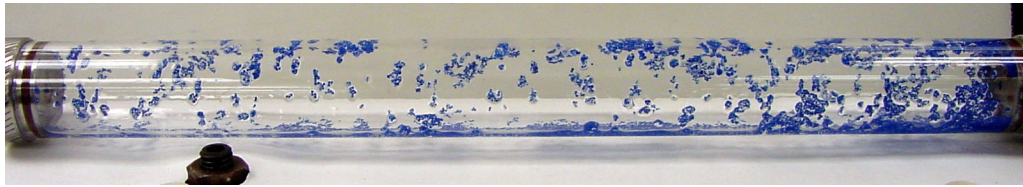
Filling level F	Rotating speed Ω (rpm)	Waiting time for particle clusters t_{w1} (hour)	Waiting time for large blocks t_{w2} (hour)	Waiting time for bands t_{w3} (hour)	Average distance between bands \bar{l} (cm)
0.061	1.76	1.1	2.6	6.6	6.2
0.061	3.13	0.8	2.1	4.7	5.5
0.061	6.00	0.6	2.2	4.0	3.9
0.061	10.0	0.5	1.8	3.5	4.5
0.046	38.71	0.10	0.25	0.40	3.9
0.046	51.10	0.08	0.20	0.30	3.6

Table 4. Times and distance of cluster and band formation.

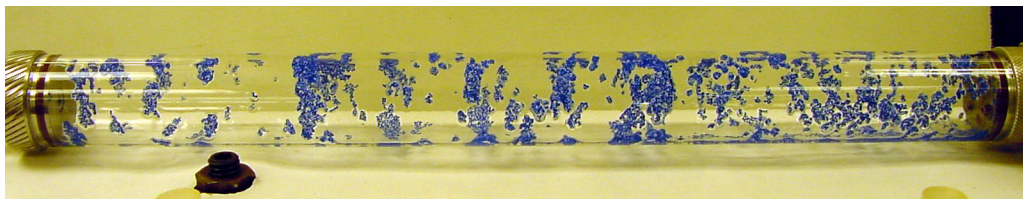
In this section we described cluster and band formation due to capillarity for lighter-than-liquid polymer particles in small concentrations in a highly viscous Triton mixture under conditions in which $D_{min}/d_p = O(1)$.

II-3. Particle segregation in water

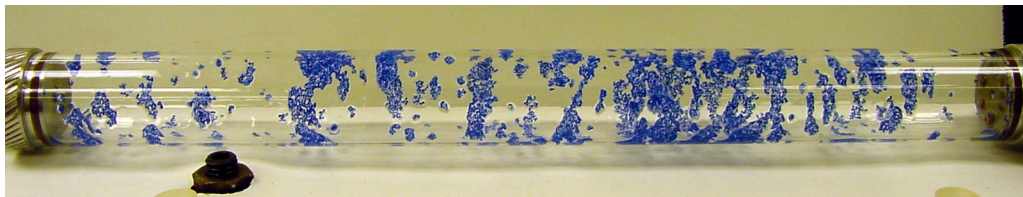
We did experiments in water using the same polymer particles as before. In figure 14 we show cluster and band formation due to capillarity for heavier-than-water particles in large concentration 20.7% with $\beta = 15.94$.



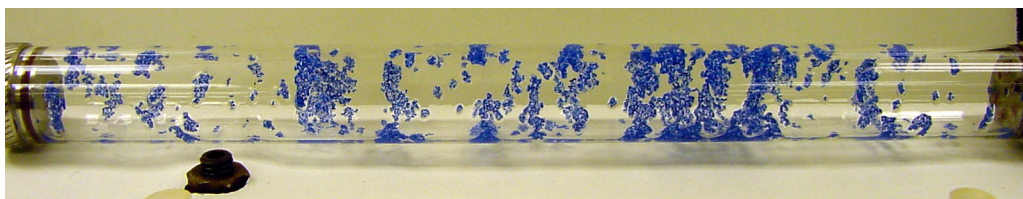
(a) 3 minutes after beginning of rotation



(b) 1.5 hours after beginning of rotation



(c) 6 hours after beginning of rotation



(d) 18 hours after beginning of rotation

Figure 14. Band formation of particles due to capillarity. The fluid is water (18°C) and the particles are polymer particles with a density of 1.034 g/cm^3 and a diameter of 0.065 cm . The filling level of the fluid is 4.08% and the particle concentration is 20.7% . The rotating speed $\Omega = 8.57\text{ rpm}$, $\beta = 15.94$, average film thickness $D_a = 0.288\text{ mm}$, minimum film thickness $D_{\min} = 0.0213\text{ mm}$, $D_{\min}/d_p = 0.033$.

II-4. Particle segregation in glycerin

Clustering and band formation due to capillarity is very robust in thin films on the inside of a rotating cylinder. In figures 15, 16 and 17 we show clusters and bands for three different cases.

In figure 15 the neutrally buoyant particles are very large and the concentration of particles is 54.2%. In figure 16 the particles are much heavier than glycerin, but bands form nonetheless. In figure 17 the particles are lighter than glycerin and bands form as well.



Figure 15. Clustering of particles due to capillarity. The fluid is glycerin with a density of 1.173 g/cm^3 , a viscosity of 1490 cp , and a surface tension of 41.46 mN/m . The particles are white Nylon particles with a density of 1.170 g/cm^3 and a diameter of 0.314 cm . The filling level of the fluid is 8.2% and the particle concentration is 54.2% . The rotating speed $\Omega=5.45 \text{ rpm}$, $\beta=1.127$, average film thickness $D_a=0.585 \text{ mm}$, minimum film thickness $D_{\min}=0.526 \text{ mm}$, $D_{\min}/d_p=0.176$. Clusters of particles form about 5 minutes after starting of rotation. Bands form occasionally but are not stable.



(a) 2.5 hours after beginning of rotation.



(b) 16 hours after beginning of rotation.

Figure 16. Band formation of particles due to capillarity. The fluid is glycerin with a density of 1.173 g/cm^3 , a viscosity of 1490 cp , and a surface tension of 41.46 mN/m . The particles are 16/20 Naplite sands with a density of 2.59 g/cm^3 and a diameter of 0.959 mm . The filling level of the fluid is 7.85% and the particle concentration is 13.0% . The rotating speed $\Omega=5.45 \text{ rpm}$, $\beta=1.079$, average film thickness $D_a=0.559 \text{ mm}$, minimum film thickness $D_{\min}=0.506 \text{ mm}$, $D_{\min}/d_p=0.528$.

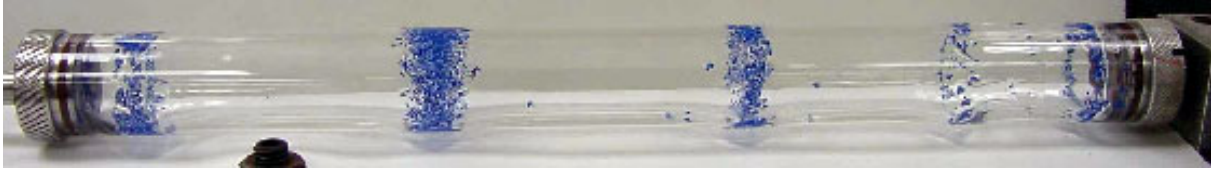


Figure 17. Band formation of particles due to capillarity. The fluid is glycerin with a density of 1.173 g/cm^3 , a viscosity of 1490 cp , and a surface tension of 41.46 mN/m . The particles are polymer particles with a density of 1.034 g/cm^3 and a diameter of 0.65 mm . The filling level of the fluid is 10.5% and the particle concentration is 4.8% . The rotating speed $\Omega = 5.45 \text{ rpm}$, $\beta = 1.443$, average film thickness $D_a = 0.753 \text{ mm}$, minimum film thickness $D_{min} = 0.605 \text{ mm}$, $D_{min}/d_p = 0.931$. Band formation 15 hours after beginning of rotation is shown in the figure.

III. Particle segregation due to the formation of bubbles:

When a partially filled horizontal cylinder is rotated at rates which are not too high or too low, the effects of surface tension and gravity are important and air bubbles separated by disks of liquid will form. The bubbles are then not centered and can take different shapes depending on conditions. The off-center bubbles pump the liquid to form the secondary motion which is from the bubble to the liquid disks near the bubble surface and from the liquid disks to the bubble near the wall (see figure 20). Particles are centrifuged to the wall if they are heavier than the liquid; they are centrifuged to the surface of the bubble if they are heavier than the air but lighter than the liquid. Driven by the secondary motion, lighter-than-liquid particles segregate in the liquid disks; heavier-than-liquid particles segregate in the region circling the bubbles when the bubbles are off the wall, and in the liquid disks when the bubbles touch the wall.

III-1. Bubbles in a partially filled rotating cylinder:

Rimming flow is a coating flow inside a partially filled rotating horizontal cylinder. The filling level F is the volume fraction of liquid in the cylinder; when F is large there is very little air in the cylinder. If the filling fraction is not too small, air bubbles will form and the shape, numbers and position of these bubbles depend on F , the angular velocity Ω , the surface tension γ , the viscosity of the liquid, the density difference between liquid and gas $\rho_l - \rho_g$, and the dimensions of the apparatus. The qualitative effects of all these parameters are fairly well understood.

When the cylinder rotates so fast that the effects of centrifugal gravity $\Omega^2 R$ (R is the cylinder radius) overwhelm those of terrestrial gravity, $\Omega^2 R/g \gg 1$, all of the liquid is centrifuged and

rotates with the cylinder as a rigid body; in this case the air is centered and if the filling level is not too small, bubbles will form under the action of an interfacial potential (see Preziosi and Joseph 1987). An important parameter for this potential is

$$J = \frac{(\rho_l - \rho_g)\Omega^2 R^3}{\gamma} \quad (20)$$

which does not depend on gravity, viscosity, filling level or the length of the apparatus. If $J < 4$ cigar shaped bubbles will form; the bubbles are all identical but the number of them depends on the filling level and the history of their creation. $J = 4$ is a limiting value for the drop shape parameters; when Ω is increased, the maximum radius of the bubble decrease in such a way that $J = 4$; when the ratio of bubble length to radius $L/R > 8$, the bubble shape is very closely approximated by a cylinder of constant radius R bounded by two semi-spherical end caps (this is nearly achieved in figure 18f).

Equation $J = 4$ was derived from heuristic arguments by Vonnegut (1942). It is the working formula for “spinning drop” tensiometer which are used to measure interfacial tension (see Joseph *et al.* 1992).

As Ω is increased, R decreases with $J = 4$. Since the bubble volume is fixed the length L increases and eventually all the bubbles collect end to end to form a long cylindrical column, rigorously centered, which does not change under further increases of angular velocity.

Coming the other way, decreasing from large values of $\Omega^2 R/g$, the length of the bubbles will decrease and the maximum radius will increase with $J = 4$. Eventually, when $\Omega^2 R/g = O(1)$ the effect of terrestrial gravity becomes important, the bubble rise; secondary motions are generated and velocity becomes important. Photographs which exhibit typical regimes are displayed in figure 18 where we compare soybean oil whose viscosity is 282 cp with Triton mixture whose viscosity is 2950 cp. The main effect of viscosity here is to maintain rigid motion of the fluid under perturbations with gravity. The radius of the cylinder used in our experiments is 0.64 cm and the ratio of centrifugal to terrestrial gravity are listed below:

Ω	200	300	600	1000
$\Omega^2 R/g$	0.287	0.64	2.57	7.16

Table 5. Gravity ratio for different angular velocity.

When $\Omega = 1000$ rpm, the bubble is rigorously centered and extends from end to end of the cylinder. When $\Omega = 600$ rpm, the effects of gravity are sensible. The perturbation of rigid motion in the high viscosity Triton mixture is small and the secondary motions are much weaker than in soybean oil. The configuration in figure 18(f) is essentially uninfluenced by gravity with centered bubbles whose shape is determined by a potential lined up end to end. At lower value of Ω , the bubbles rise but the secondary motions which distort the bubbles are less important in the high viscosity fluid.

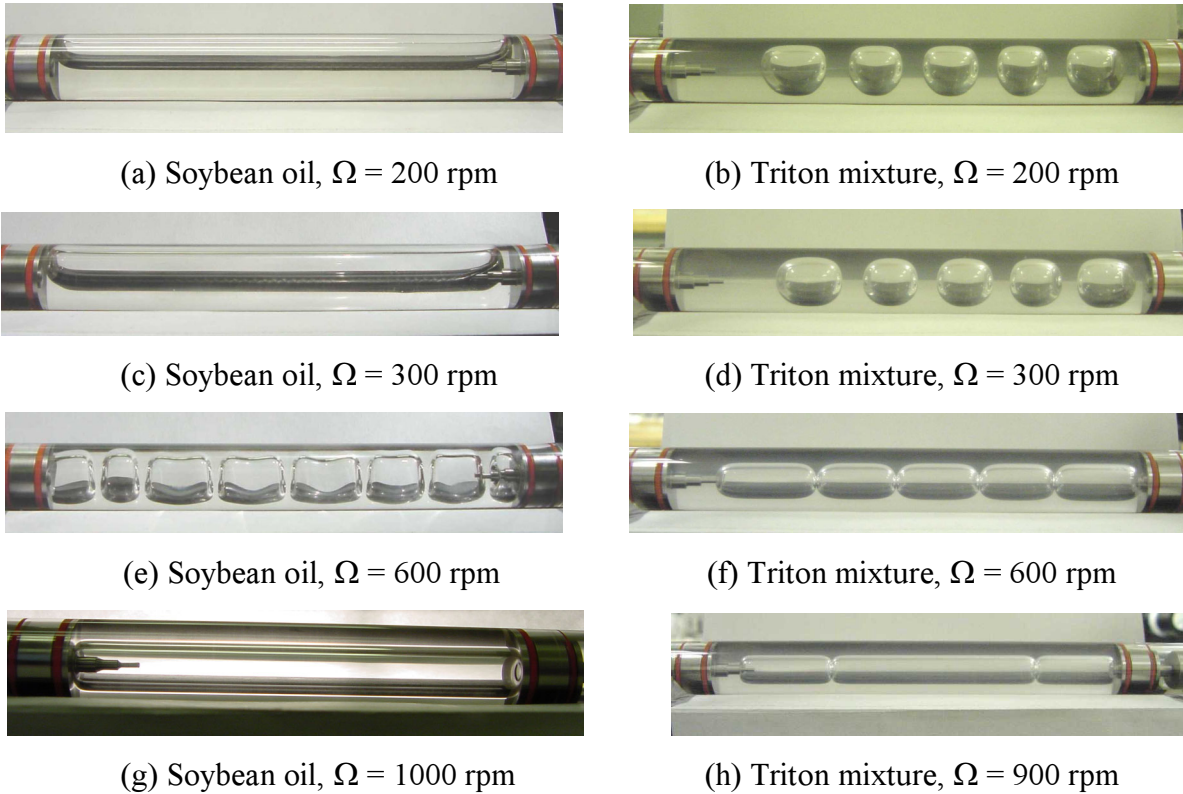


Figure 18. Comparison of soybean oil and Triton mixture under same conditions

As the angular velocity is decreased to zero the liquid and air stratify, with all the air at the top. Even in this case, a stationary fluid, the air may separate into bubbles induced by capillarity if the filling level is not very high; if the filling level is near 100%, the very small amount of air will rise to the top and form a single short bubble due to the restraining action of surface tension.

Many unusual shapes of bubbles may occur when $\Omega^2 R/g$ is not too large as put into evidence and in the papers by Balmer (1970), Joseph and Beavers (1981) and Preziosi and Joseph (1988).

The combined effects of the filling level and rotational speed are of interest. When the gravity ratio parameter is small the liquid and air are stratified even though a thin film is dragged up by the rotating cylinder. If the filling level is large enough, the thickness of the film dragged up increases. Up to a critical condition, the uniform liquid film cannot be maintained and part of it falls down under gravity, subsequently the single air bubble breaks. On the other hand, when the gravity ratio parameter is large, the air forms a rigorously centered cylindrical column stretching from end to end of the cylinder. If the rotational speed decreases, the stabilizing effect of the centrifugal acceleration decreases. Up to a point, the combined effects of the surface capillarity and the terrestrial gravity will break up the air bubble into smaller ones.

The critical conditions under which air bubble separation happens were determined experimentally for the rimming flow of soybean oil. The two lines on a (F, Ω) plane in figure 19 indicate the critical conditions. When the filling level and rotational speed fall in the region between the two lines, bubble separation is observed; otherwise, a single air bubble is stable. Note that when $F < 0.4$, bubble separation does not happen at any rotational speed.

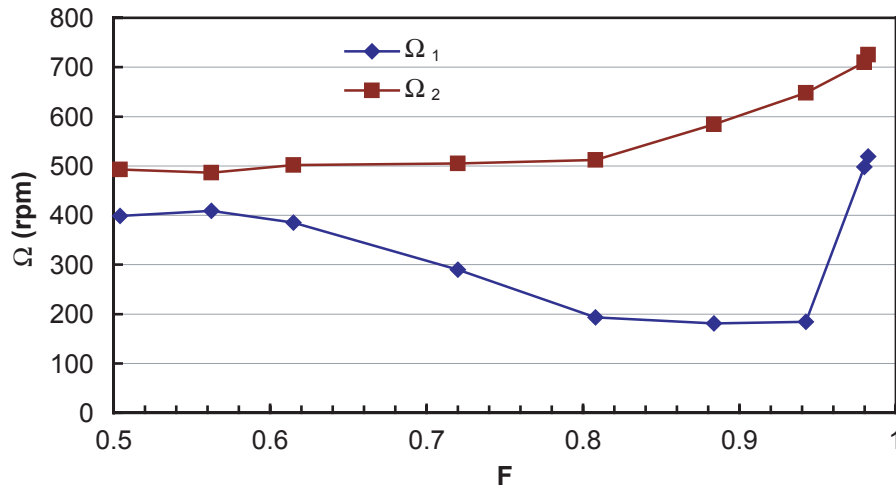


Figure 19. Critical conditions for air bubble separation in soybean oil. The experiments were carried out in a cylinder of glass with inside diameter 1.28 cm and length 22.14 cm. When $F < 0.4$, bubble separation does not happen at any rotational speed. For $F \geq 0.5$, when the rotational speed is larger than Ω_1 but smaller than Ω_2 , air bubble separation is observed.

III-2. Particles segregation due to bubbles:

The motion of the particle is driven by the secondary motions associated with the pumping motion of off-center bubbles. The liquid passes by the above-center bubbles which are relatively

stationary and are pushed away from the places occupied by the air. The pumping motion of the bubble sets up an eddy which will push the liquid from the bubble to the liquid disks near the bubble surface and from the liquid disks to the bubble near the wall (see figure 20).

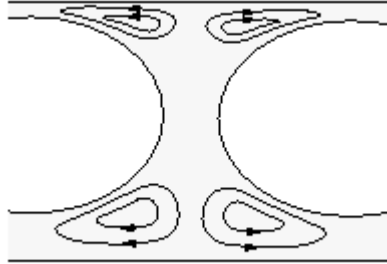
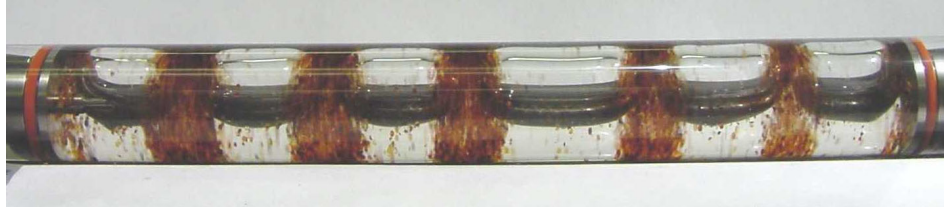


Figure 20. The eddies set up by the pumping motion of the off-center bubble. Liquid flows from the bubble to the liquid disks near the bubble surface and from the liquid disks to the bubble near the wall.



(a) $\Omega = 200$ rpm



(b) $\Omega = 300$ rpm



(c) $\Omega = 600$ rpm



(d) $\Omega = 1000$ rpm

Figure 21. Particle segregation of resin particles $\rho_p = 1.13$ g/cm, average diameter $d_p = 0.065$ cm, concentration 15% in soybean oil, filling level 60%.

The changes in the nature of heavier-than-liquid particle segregation as $\Omega^2 R/g$ changes (see table 5) are shown in four panels of figure 21 where we go from stratified flow (a) to uniform flow (d). The experiments were carried out in a cylinder of glass with inside diameter 1.28 cm and length 22.14 cm. Comparing figure 18(a, c) with figure 21(a, b) we see that the particles promote bubble formation at low speeds in soybean oil. This effect may be due to the increase in the effective density of the mixture which increases the value of J in (20) by replacing ρ_l with $\rho_c = \rho_p \phi + \rho_l(1 - \phi)$ where ϕ is the particle fraction.

The heavier-than-liquid particles are centrifuged and segregated near the cylinder wall where secondary motions are weakest. The eddies push the particles on the wall to the region circling

the bubble and away from the gap between bubbles when the rotational speed of the cylinder is large enough to centrifuge the air away from the wall but not so large as to center it (figure 21c). At lower speeds, the bubbles rise all the way to the wall and the particles on the wall are pushed to the space between bubbles (figure 21a,b).

In figure 22 we show that for heavier-than-liquid particles, segregation does not depend sensitively on the type of particle when the particle properties are not too different.

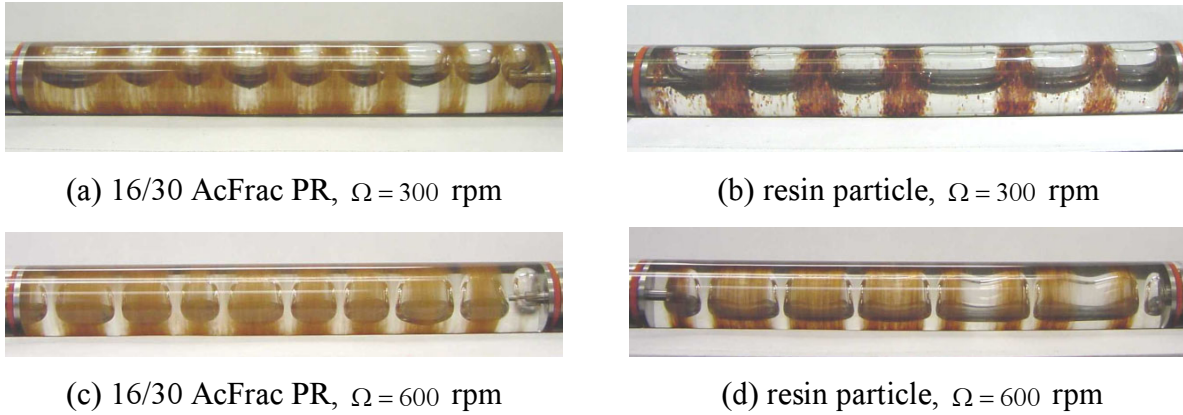


Figure 22. Particle segregation in soybean oil under conditions specified in the caption to figure. The AcFrac PR particles are hydrophilic, $\rho_p = 1.64 \text{ g/cm}^3$, average diameter $d_p = 0.088 \text{ cm}$; the resin particles are hydrophobic, $\rho_p = 1.13 \text{ g/cm}^3$, average diameter $d_p = 0.065 \text{ cm}$.

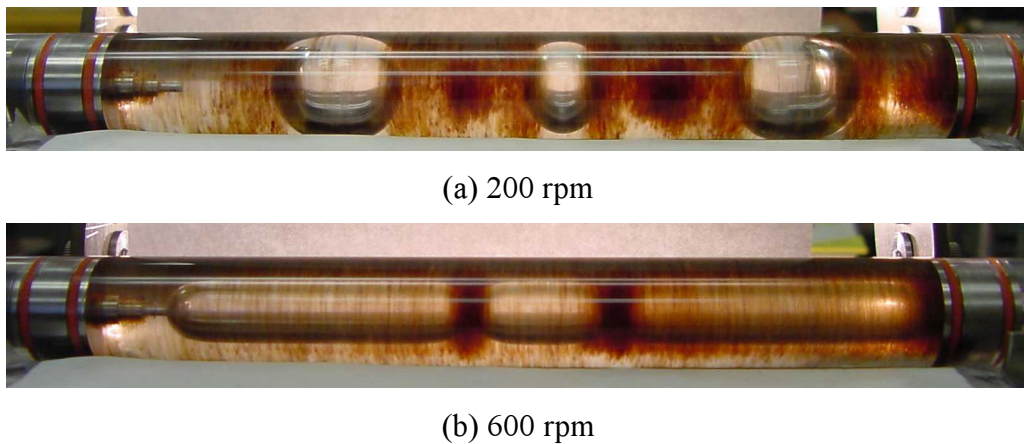


Figure 23. Particle segregation of resin particles $\rho_p = 1.13 \text{ g/cm}^3$, average diameter $d_p = 0.065 \text{ cm}$, concentration 8.96% in glycerin, filling level 66.7%.

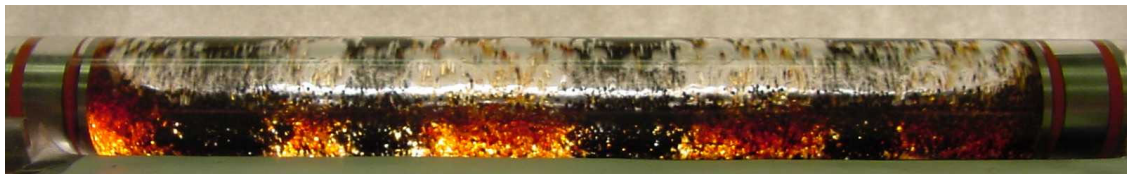
Figure 23 shows the segregation pattern of particles which are heavier than the air but lighter than the liquid. The lighter-than-liquid particles are centrifuged to the surface of the bubbles. The eddies described in figure 20 will push the particles to the space between air bubbles. Compare figure 21(c) with figure 23(b), the different patterns should be noted. The heavier-than-liquid

particles segregate in the region above the bubbles, whereas the lighter-than-liquid particles segregate in the space between bubbles. In figure 23(b), some of particles do circulate around the bubbles because the bubbles are almost centered and the secondary motions are weak.

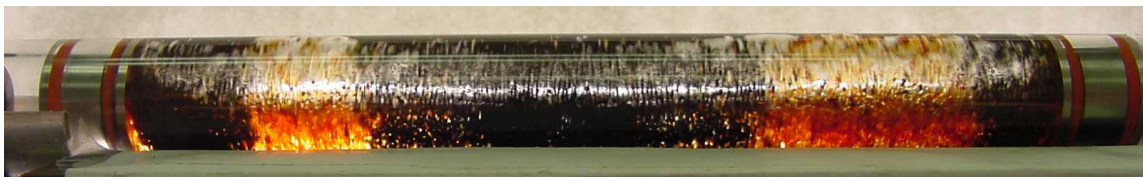
III-3. Segregation of bi-disperse suspension in a partially filled rotating cylinder

Preliminary experiments using suspensions of particles with two different weights show that the rotating flow leads to segregation of the two types of particles into separate regions whose exact form depends on the weight and concentration of particles and on other features which have yet to be determined. Here we show that this kind of segregation does occur and is robust.

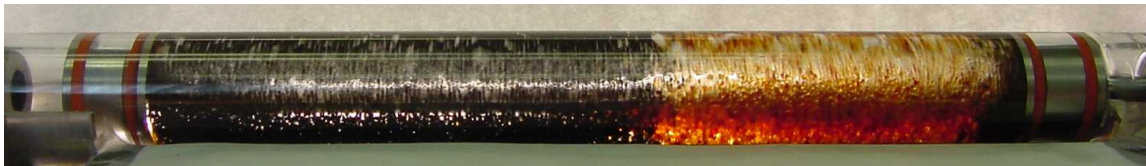
Figure 24 and 25 show two experiments of segregation of bi-disperse suspension in aqueous glycerin solutions. The different concentrations of the brown resin particles cause different patterns of segregation (figure 24a and figure 25a). The rotating flow finally leads to uniform distribution of particles, with the heavy particles at the end of the cylinder and the light particles at the middle of the cylinder (figure 24c and figure 25c). Figure 26 shows bi-disperse suspension in water. The configuration shown in figure 26 is stable for hours.



(a) 30 minutes after beginning of rotation.



(b) two hours after beginning of rotation.

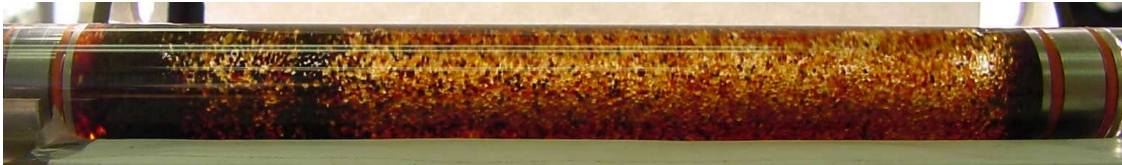


(c) 20 hours after beginning of rotation.

Figure 24. Segregation of two types of particles in a 47.8% aqueous glycerin solution, $\rho_l = 1.09 \text{ g/cm}^3$. The filling level of the liquid is 0.354. The black is a silicon particle with $\rho_p = 3.07 \text{ g/cm}^3$, average diameter $d_p = 0.05 \text{ cm}$, and its concentration is 21.7%. The brown is a resin particle with $\rho_p = 1.13 \text{ g/cm}^3$, average diameter $d_p = 0.065 \text{ cm}$, and its concentration is 12%. The rotational speed is 165 rpm.



(a) four minutes after beginning of rotation.



(b) 24 minutes after beginning of rotation.



(c) 36 minutes after beginning of rotation.

Figure 25. Segregation of two types of particles in a 48.7% aqueous glycerin solution. The filling level of the liquid is 0.328. The black is a silicon particle with $\rho_p = 3.07 \text{ g/cm}^3$, average diameter $d_p = 0.05 \text{ cm}$, and its concentration is 16%. The brown is a resin particle with $\rho_p = 1.13 \text{ g/cm}^3$, average diameter $d_p = 0.065 \text{ cm}$, and its concentration is also 16%. The rotational speed is 160 rpm.



Figure 26. Segregation of two types of particles in water. The filling level is 0.357. The black is a silicon particle with $\rho_p = 3.07 \text{ g/cm}^3$, average diameter $d_p = 0.05 \text{ cm}$, and its concentration is 4%. The brown is a resin particle with $\rho_p = 1.13 \text{ g/cm}^3$, average diameter $d_p = 0.065 \text{ cm}$, and its concentration is 16%. The rotational speed is 306 rpm.

IV. Conclusion

The principal facts concerning capillary attraction and self-assembly of small lighter- and heavier-than-fluid floating particles were reviewed. These facts were applied to explain the clustering and segregation of bands of particles in a thin liquid film rimming the inside of a partially filled, slowly rotating cylinder in situations resembling those first observed by Tirumkudulu, Mileo and Acrivos (2000). In our experiments clustering and band formation occurred under all kinds of conditions, for lighter- and heavier-than-liquids, for small particles

and large particles, and for low concentrations and high concentrations of particles. Uniform dispersions of particles in thin films are robustly unstable to anti-diffusion due to capillarity, and clusters which are self-assembled are robustly stable. The conditions required to support this phenomenon are that the liquid film is thin relative to the particle size; the film should be thin, or in any case, not much thicker than the particles. The rotation speed of the cylinder should be slow enough that the time needed for sensible capillary attraction is comparable to the time of residence of the particle in the thin part of the rimming film.

Particle segregation may also be generated by pumping secondary motions of fluid by off-center gas bubbles, which arise when the gravity parameter $\Omega^2 R/g \leq O(1)$ and the filling level is not too small. Lighter-than-liquid particles segregate in the liquid disks between bubbles; heavier-than-liquid particles segregate in the region above the bubbles when they are off the wall, and in the liquid disks when the bubbles touch the wall.

A third regime of segregation of bidisperse suspension of particles of different heavier-than-liquid weights, which stratify when the cylinder is at rest, form into rings when the cylinder rotates. Different forms of the ring appear to depend on the particle concentration and other factors which have as yet to be determined.

Acknowledgement

The work of authors Joseph, Wang, Bai and Yang was supported by the NSF/CTS under grant 9873236, and by the Engineering Research Programs at the Office of Basic Energy Science of the DOE.

References

- Balmer, R.T. The hydrocyst—a stability phenomenon in continuum mechanics, *Nature* (London) **227**, 600 (1970).
- Bowden, N., I.S. Choi, B.A. Grzybowski, G.M. Whitesides, Mesoscale self-assembly of hexagonal plates using lateral capillary forces: synthesis using the “capillary bond”, *J. Am. Chem. Soc.* **121**, 5373-5391. (1999).
- Bowden, N., A. Terfort, J. Carbeck, G.M. Whitesides, Self-assembly of mesoscale objects into ordered two-dimensional arrays, *Science*, **276**, 233-235. (1997).
- Brenner, H. and L.G. Leal. A micromechanical derivation of Fick’s law for interfacial diffusion of surfactant molecules, *J. Colloid Interface Sci.* **65**, 191 (1978).
- Brenner, H. and L.G. Leal. Conservation and constitutive equations for adsorbed species undergoing surface diffusion and convection at a fluid-fluid interface, *J. Colloid Interface Sci.* **88**, 136 (1982).
- Chan, D.Y.C., J.D. Henry Jr. and L.R. White. The interaction of colloidal particles collected at the fluid interface, *J. Colloid Interface Sci.* **79**, 410 (1981).
- Danov, K.D., R. Aust, F. Durst and U. Lange. Influence of the surface viscosity on the hydrodynamic resistance and surface diffusivity of a large Brownian particle, *J. Colloid and Interface Science*, **175**(1), Oct 36-45 (1995).
- Fortes, M.A. Attraction and repulsion of floating particles, *Can. J. Chem.* **60**, 2889 (1982).
- Gifford, W.A. and L.E. Scriven. On the attraction of floating particles, *Chem. Engrg. Sci.* **26**, 287-297 (1971).
- Goldman, A.J., R.G. Cox and H. Brenner. Slow viscous motion of a sphere parallel to a plane wall—I Motion through a quiescent fluid, *Chem. Eng. Sci.* **22**, 637-651 (1967).
- Govindarajan, R., P.R. Nott, and S. Ramaswamy. Theory of suspension segregation in partially filled horizontal rotating cylinders, *Phys. Fluids*, **13**(12), 3517-3520 (2001).
- Grzybowski, B.A., N. Bowden, F. Arias, H. Yang, G.M. Whitesides, Modeling of menisci and capillary forces from the millimeter to the micrometer size range, *J. Phys. Chem. B* **105**, 404-412. (2001).
- Joseph, D.D., M. Arney, G. Ma, 1992. Upper and lower bounds for interfacial tension using spinning drop devices, *J. Colloid Interface Sci.*, **148**(1), 291-294.
- Karweit, M.J. and S. Corsin. Observation of cellular patterns in a partly filled, horizontal, rotating cylinder, *Phys. Fluids* **18**, 111 (1975).
- Katoh, K., H. Fujita and E. Imazu. Motion of a particle floating on a liquid meniscus surface, *J. Fluids Engrg.* **114**, 411 (1992).
- Kralchevsky, P.A., V.N. Paunov, N.D. Denkov, I.B. Ivanov and K. Nagayama. Energetical and force approaches to the capillary interactions between particles attached to a liquid-fluid interface, *J. Colloid and Interface Sci.* **155**, 420-437 (1993).

- Kralchevsky, P.A., V.N. Paunov, I.B. Ivanov and K. Nagayama. Capillary meniscus interactions between colloidal particles attached to a liquid-fluid interface, *J. Colloid Interface Sci.* **151**, 79 – 94 (1992).
- Kralchevsky, P.A. and K. Nagayama. Capillary interactions between particles bound to interfaces, liquid films and biomembranes, *Advances in Colloid and Interface Sci.* **85**, 145-192 (2000).
- Majumdar, S.R., M.E. O'Neill, and H. Brenner. Note on the slow rotation of a concave spherical lens or bowl in two immiscible semi-infinite viscous fluids, *Mathematika*, **21**, 147-154 (1974).
- Nicolson, M.M. The interaction between floating particles, *Proc. Cambridge Philosophical Soc.*, **45**, 288 (1949).
- Petkov, J.T., N.D. Denkov, K.D. Danov, O.D. Velev, R. Aust and F. Durst. Measurement of the drag coefficient of spherical particles attached to fluid interfaces, *J. Colloid and Interface Science*, **172**, 147-154 (1995).
- Poynting, J.H. and J.J. Thompson. *A Text-book of Physics: Vol. 1, Properties of Matter*, C. Griffith & Co. Ltd (London) 153-155 (1913).
- Preziosi, L. and D.D. Joseph. The run-off condition for coating and rimming flows, *J. Fluid Mech.*, **187**, 99-113 (1988).
- Princen, H.M. Equilibrium shape of interfaces, drops, and bubbles. Rigid and deformable particles at interfaces, *Surface and Colloid Science*, E. Matijevic, ed., Interscience, New York, Vol. 2, p.1-84 (1969).
- Rapacchietta, A.V. and A.W. Neumann. Force and free-energy analyses of small particles at fluid interfaces: II. Spheres, *J. Colloid and Interface Sci.*, **59**(3), 555-567 (1977).
- Redoev, B., M. Nedjalkov and V. Djakovich. Brownian motion at liquid-gas interfaces. 1. Diffusion coefficients of macroparticles at pure interfaces, *Langmuir*, **8**, 2962 (1992).
- Ruschak, K.J. and L.E. Scriven, Rimming flow of liquid in a rotating horizontal cylinder, *J. Fluid Mech.* **76**, 113-127 (1976).
- Saif, T.A., On the capillary interaction between solid plates forming menisci on the surface of a liquid, *J. Fluid Mech.* in press (2002).
- Schneider, Y.C., M.E. O'Neill, and H. Brenner. On the slow viscous rotation of a body straddling the interface between two immiscible semi-infinite fluids, *Mathematika*, **20**, 175 (1973).
- Timberlake, B.D., J.F. Morris, Concentration band dynamics in free-surface Couette flow of a suspension, *Phy. Fluids*, **14**(5), 1580-1589 (2002).
- Tirumkudulu, M., A. Tripathi, A. Acrivos. Particle segregation in monodisperse sheared suspensions, *Phy. Fluids*, **11**(3), 507-509 (1999).
- Tirumkudulu, M., A. Mileo, A. Acrivos. Particle segregation in monodisperse sheared suspensions in a partially filled rotating horizontal cylinder, *Phy. Fluids*, **12**(6), 1615 (2000).

- Tirumkudulu, A. Acrivos. Coating flows within a rotating horizontal cylinder: Lubrication analysis, numerical computations, and experimental measurements, *Phys. Fluids*, **13**, 3517 (2001).
- Vonnegut, B., Rotating Bubble Method for the Determination of Surface and Interfacial Tension, *Rev. Sci. Instrum.* **13**, 6-9, (1942).
- Wakiya, S. *Niigata Univ. College of Engng. Res. Rept. 6*, Nagoaka, Japan (30 March 1957).

Table of contents

Abstract 1

I. Capillary forces 1

I-1. Vertical forces 2

I-2. Horizontal forces 4

I-3. Particle clustering 7

II. Particle aggregation in a liquid film rimming a rotating cylinder 11

II-1. The ratio of the minimum film thickness to the particle diameter 12

II-2. Particle segregation in aqueous Triton mixtures 16

II-3. Particle segregation in water 21

II-4. Particle segregation in glycerin 21

III. Particle segregation due to the formation of bubbles: 23

III-1. Bubbles in a partially filled rotating cylinder: 23

III-2. Particles segregation due to bubbles: 26

III-3. Segregation of bi-disperse suspension in a partially filled rotating cylinder 30

IV. Conclusion 31

References 32